Gait & Posture 88 (2021) 146–154

Contents lists available at ScienceDirect

Gait & Posture

journal homepage: www.elsevier.com/locate/gaitpost

Full length article

A planar piecewise continuous lumped muscle parameter model for prediction of walking gait

Albert Qianyi Fu [a,*], Albert J. Shih [b,c], Bernard J. Martin [a], Thomas J. Armstrong [a,c]

[a] Department of Industrial and Operations Engineering, University of Michigan, Ann Arbor, MI, USA
[b] Department of Mechanical Engineering, University of Michigan, Ann Arbor, MI, USA
[c] Department of Biomedical Engineering, University of Michigan, Ann Arbor, MI, USA

ARTICLE INFO

Keywords:
Piecewise continuous model
Gait prediction
Forward dynamics
Lumped muscle parameters

ABSTRACT

Goal: This work aims to develop a planar piecewise continuous lumped muscle parameter (PPCLMP) model that can utilize inputs that can be obtained in a clinical or home setting using simple tools (e.g. video cameras and inertial sensors) to predict human walking gait.
Methods: The model characterizes the sagittal-plane movement of the lower limbs during the single stance phase as an inverted pendulum, the double stance phase as a kinematic chain, and the swing phase as a double pendulum. The joint angles and angular velocities at the end of one phase are used as the initial conditions of the next phase. The model predicts the gait cycle based on the initial joint angles and angular velocities via forward dynamics. The errors between the initial and end conditions are minimized by changing the input initial joint angles and angular velocities of the gait cycle.
Results: Sensitivity analysis showed that the errors between the initial and end conditions of a gait cycle were sensitive to the initial joint angles. The step length was sensitive to subject stature. The model only works for a certain range of initial conditions.
Conclusions: The model can predict gait cycles based on forward dynamics and selects initial conditions that minimize the errors between the initial and end conditions of the gait cycle. The model utilizes 2-D representations of lower limbs and simplified representations of joint torques to reduce the required inputs for gait prediction and builds the foundation of gait assessment tools.

1. Introduction

Gait analysis is widely used for the diagnosis of gait disorders related to motor control issues in the lower limbs, identification of underlying pathologies, and design of medical interventions [1,2]. Gait analysis typically utilizes 3D motion tracking systems to measure joint angles throughout the gait cycle. Unfortunately, this equipment and the skills to operate that equipment are not available in many clinics. Additionally, many patients can be seen by their healthcare providers remotely in their home settings. There is a need for simple models that can utilize readily available tools such as inertial measurement units (IMUs) and video cameras that are built into most smartphones and smartwatches to obtain and interpret gait patterns.

Gait is commonly divided into four phases: one single stance phase (SS), two double stance phases (DSs), and one swing phase (SW). Detailed biomechanical models have been built to characterize the leg movements in SS, DSs, and SW. The SS was characterized by the inverted pendulum model with the leg rotating about the ankle joint [3]. The DS was characterized by a kinematic chain model with both feet constrained on the ground [4]. The SW was characterized by a double pendulum model with the upper leg as the upper pendulum and the lower leg as the lower pendulum [5,6]. Approaches have been made to merge these models of different gait phases to perform energy-based predictive gait simulations by tuning muscle contractile and activation elements to minimize energy expenditure [7,8]. However, these approaches tend to be computationally expensive and require inputs from complicated tools.

The goal of this paper is to develop a simplified planar piecewise continuous lumped muscle parameter (PPCLMP) model for describing the entire gait cycle. The model merges and builds on the existing models for SS, DSs, and SW to describe and predict complete gait cycles via forward kinematics. Model applications include the study of

* Corresponding author.
E-mail address: qifu@umich.edu (A.Q. Fu).

https://doi.org/10.1016/j.gaitpost.2021.05.021
Received 19 August 2020; Received in revised form 14 May 2021; Accepted 20 May 2021
Available online 24 May 2021

pathological gait and gait with and without assistive devices.

2. The PPCLMP model

The proposed PPCLMP model is developed to explore the simplification of muscle activities and the importance of gait initial conditions in predicting human gait. The model is based on an inverted pendulum model, a kinematic chain model, and a double pendulum model that correspond to SS, DS, and SW, respectively. The joint angles and angular velocities at the end of each phase are used to determine the initial conditions of the next phase.

The flowchart of the model is shown in Fig. 1(a). Along with the initial conditions, the additional inputs of the model are anthropometry data, and preset generic lumped muscle parameters. The model predicts gait parameters via forward kinematics based on the inputs.

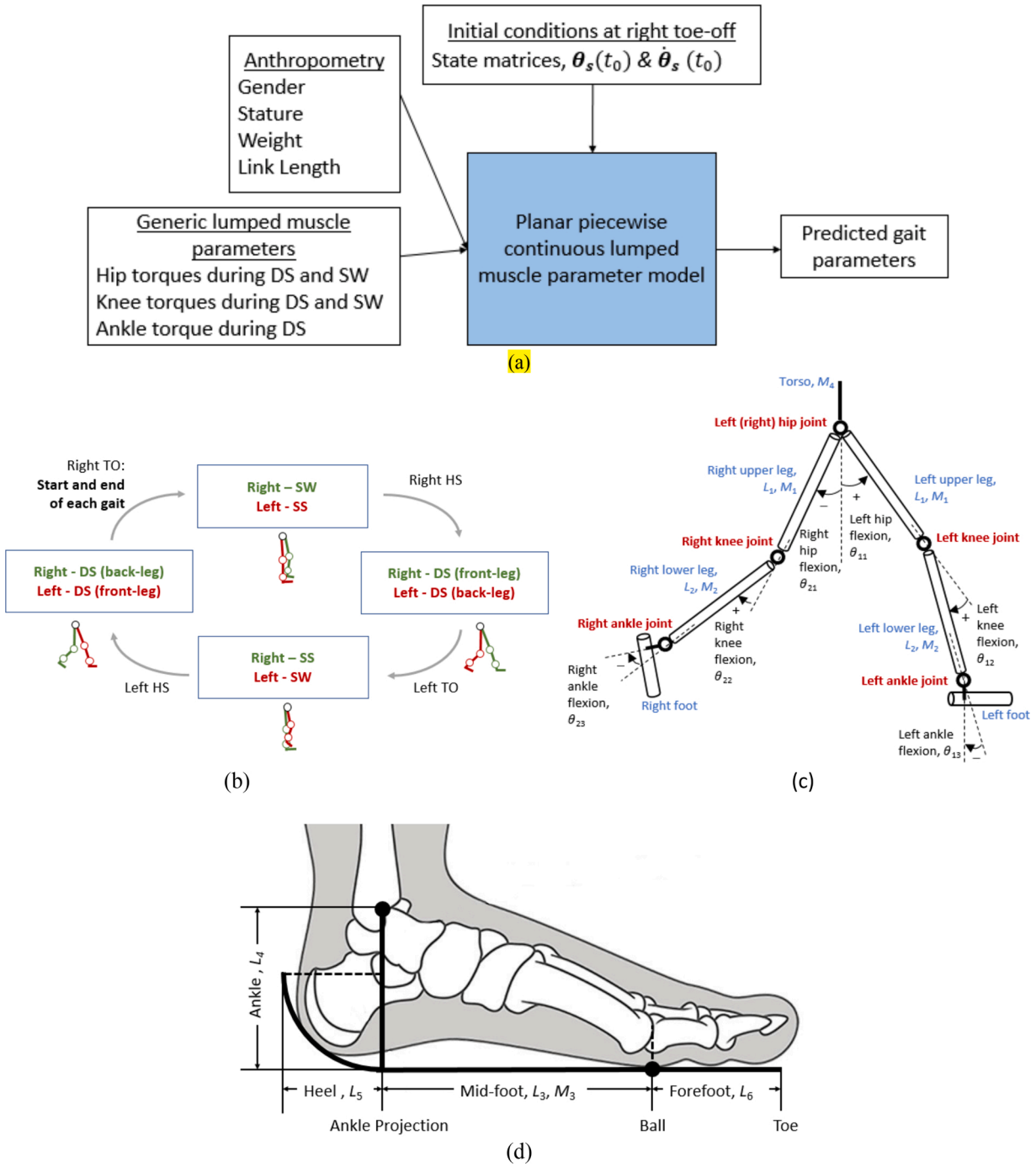

Fig. 1. (a) Flowchart of the proposed PPCLMP model for predicting gait parameters; (b) The phases and events of the right (green) and left (red) legs during a gait cycle: the gait starts from the right TO, then to the right SW and left SS, then to the right HS, then to the DS (right leg in front), then to the left TO, then to the right SS and left SW, then to the left HS, then to the DS (right leg in the back), and then back to the right TO (start of the gait); (c) biomechanical model with definitions of limb links, joints, and joint angles in the sagittal plane; and (d) the foot anatomy and dimensions in the sagittal plane (part of the image adopted from https://www.hss.edu/conditions_common-conditions-foot-ankle-overview.asp on February 2, 2020). (For interpretation of the references to colour in this figure legend, the reader is referred to the web version of this article).

2.1. The musculoskeletal model

Fig. 1(b) illustrates the sequence of gait phases with toe-offs (TOs) and heel strikes (HSs) as the beginning and end of the gait phases. The planar link system of the lower limbs [9] adopted for this study is shown in Fig. 1(c). The system contains six body segments and six hinge joints. Body segments are represented as symmetric (right-left) rod links with lengths (L_i) and uniformly distributed masses (M_i). The whole foot link is rigid with its dimensions characterized by the rocker model [10], as shown in Fig. 1(d).

2.1.1. Body links and joint angles

The length of the link i can be determined from direct measurements of subjects or estimated based on published link-length ratios [11]:

$$L_i = L_0 l_i \quad (1)$$

where l_i is the link-length ratio of link i (Table 1) and L_0 is the measured stature of the subject. Similarly, the mass of link i denoted as M_i follows:

$$M_i = M_0 m_i \quad (2)$$

where m_i is the mass-ratio of link i (Table 1) and M_0 is the measured body mass.

The joint angles are denoted as θ_{ij} where i represents the side (1 for left and 2 for right) and j represents the joint (1 for hip, 2 for knee, and 3 for ankle) as shown in Fig. 1(c). All the angles are measured from the standing neutral posture angles. Flexion directions (dorsiflexion for ankle joint) are considered positive, and extension directions (plantar flexion for ankle joint) are considered negative.

2.1.2. Lumped muscle parameters

It is assumed that the adjacent links are connected by a hinge joint where torques generated by muscles are simplified and lumped into one joint torque that linearly changes with the associated joint angle based on the reported joint torques and angles during gait from Winter [12]. This linear relationship is characterized by the lumped muscle parameters (stiffness of a rotational spring), k_{ijp}, in Nm/deg, where i represents the side (1 for left and 2 for right), j represents the joint (1 for hip, 2 for knee, and 3 for ankle), and p represents the phase (1 for SS, 2 for DS, and 3 for SW). Due to the different joint torque patterns of the ankle during DS [12], the ankle torque during DS is characterized by the lumped muscle parameter, r_{i32}, in Nm per kg body mass. A summary of the lumped muscle parameters used in the planar link system is listed in Table 1. The biomechanical models of the three phases are described in the following sections.

2.2. Single stance phase

As shown in Fig. 1(b), the SS of one side starts at the TO of the other side and ends at the HS of the other side. An inverted pendulum model is used to predict the leg movement during the SS (Fig. 2(a)). The upper leg and lower leg are rotating about the ankle joint with the knee being

Table 1
The link-length ratios, link-mass ratios, and lumped muscle parameters for model inputs, and the range of initial condition, and anthropometry for sensitivity analysis.

		Parameters	i	Link length ratios*, l_i	
				Male	Female
Model Defaults	Anthropometry data	Stature		1	1
		Upper leg length	1	0.257	0.254
		Lower leg length	2	0.229	0.230
		Ankle height	3	0.042	0.039
		Forefoot length	4	0.026	0.039
		Mid-foot length	5	0.1	0.09
		Heel length	6	0.03	0.03

		Parameters	i	Link mass ratios*, m_i	
				Male	Female
Model Defaults	Anthropometry data	Body mass		1	1
		Upper leg mass	1	0.132	0.135
		Lower leg mass	2	0.044	0.046
		Foot mass	3	0.014	0.013
		Upper body mass	4	0.62	0.61
	Lumped muscle Parameters**	Phase	Joint (i = 1 and 2)	Value	
		DS	Hip, k_{i12} (Nm/deg)	20	
			Knee, k_{i22} (Nm/deg)	20	
			Ankle, r_{i32} (Nm/kg)	1.5	
		SW	Hip, k_{i13} (Nm/deg)	20	
			Knee, k_{i23} (Nm/deg)	8	

	Type	Parameters	Unit	Range (start, stop, step)	Valid Range
Sensitivity Analysis	Initial conditions	$\theta_{11}(t)$	Deg	(5, 30, 5)	(5, 30)
		$\theta_{21}(t)$	Deg	(–5, –30, –5)	(-5, –10)
		$\theta_{22}(t)$	Deg	(20, 45, 5)	(25, 45)
		$\dot{\theta}_{11}(t)$	Deg/s	(–100, –200, –50)	(–100, –200)
		$\dot{\theta}_{21}(t)$	Deg/s	(25, 275, 50)	(75, 175)
		$\dot{\theta}_{22}(t)$	Deg/s	(75, 275, 50)	(125, 275)

	Type	Parameters	Unit	Values to be tested
Sensitivity Analysis	Gender	–	–	M, F
	Stature	L_0	m	1.51, 1.70, 1.88
	Body mass	M_0	kg	51, 88, 125

* The link-length ratios are from ANSUR II [11]. The heel ratio is separately estimated based on data reported by Hansen et al. [10]. The link mass ratios are from Drillis and Contini [24].

** The lumped muscle parameters of the hip and knee joints describe the joint torques by spring stiffness. The ankle torque is a constant function of body mass.

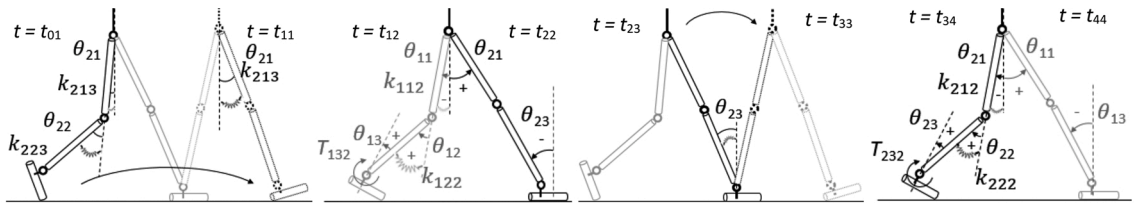

(a) SS ($t = t_{01} \rightarrow t_{11}$) (b) DS ($t = t_{12} \rightarrow t_{22}$) (c) SW ($t = t_{23} \rightarrow t_{33}$) (d) DS ($t = t_{34} \rightarrow t_{44}$)

Time	t_0	$t_{01} \rightarrow t_{11}$	t_1	$t_{12} \rightarrow t_{22}$	t_2	$t_{23} \rightarrow t_{33}$	t_3	$t_{34} \rightarrow t_{44}$	$t_4 = t_0$
Right	TO	SW Eqs. (5) and (6) Inertial and muscle forces	HS	DS (front leg) (Appendix A) Inertial forces		SS Eq. (3) Inertial forces		DS (latter leg) (Appendix A) Inertial and muscle forces	TO
Left		SS Eq. (3) Inertial forces		DS (latter leg) (Appendix A) Inertial and muscle forces	TO	SW Eqs. (5) and (6) Inertial and muscle forces	HS	DS (front leg) (Appendix A) Inertial forces	
State vector Eq. (6)	$\boldsymbol{\theta}_s(t_0)$ $\dot{\boldsymbol{\theta}}_s(t_0)$	$\boldsymbol{\theta}_s(t_{01}) \rightarrow \boldsymbol{\theta}_s(t_{11})$ $\dot{\boldsymbol{\theta}}_s(t_{01}) \rightarrow \dot{\boldsymbol{\theta}}_s(t_{11})$	$\boldsymbol{\theta}_s(t_1)$ $\dot{\boldsymbol{\theta}}_s(t_1)$	$\boldsymbol{\theta}_s(t_{12}) \rightarrow \boldsymbol{\theta}_s(t_{22})$ $\dot{\boldsymbol{\theta}}_s(t_{12}) \rightarrow \dot{\boldsymbol{\theta}}_s(t_{22})$	$\boldsymbol{\theta}_s(t_2)$ $\dot{\boldsymbol{\theta}}_s(t_2)$	$\boldsymbol{\theta}_s(t_{23}) \rightarrow \boldsymbol{\theta}_s(t_{33})$ $\dot{\boldsymbol{\theta}}_s(t_{23}) \rightarrow \dot{\boldsymbol{\theta}}_s(t_{33})$	$\boldsymbol{\theta}_s(t_3)$ $\dot{\boldsymbol{\theta}}_s(t_3)$	$\boldsymbol{\theta}_s(t_{34}) \rightarrow \boldsymbol{\theta}_s(t_{44})$ $\dot{\boldsymbol{\theta}}_s(t_{34}) \rightarrow \dot{\boldsymbol{\theta}}_s(t_{44})$	$\boldsymbol{\theta}_s(t_4)$ $\dot{\boldsymbol{\theta}}_s(t_4)$

Fig. 2. Summary of state vectors transferred between phases and forces and equations related to each phase. Top diagrams represent the joint angles and lumped muscle parameters related to the right leg (solid black) movement during each phase: (a) The right leg movement during the SW is simulated by a double-pendulum with two rotational springs at the knee and hip joints, from right TO (t_0) to right HS (t_1), (b) the leg movements during the DS are simulated by a kinematic chain model with the right leg in front, from right HS (t_1) to left TO (t_2), (c) the right leg movement during the SS is simulated by an inverted pendulum, from left TO (t_2) to left HS (t_3), and (d) the leg movements during the DS are simulated by a kinematic chain model with the right leg in the back, from left HS (t_3) to right TO (t_4).

straight. By assuming the knee is straight and the foot is flat on the ground during SS, the equation of motion for the inverted pendulum can be adapted from [6] as:

$$\ddot{\theta}_{i1} = \ddot{\theta}_{i3} = \frac{6g(M_1L_1 + M_2L_2 + 2M_1L_2 + 2M_4(L_1 + L_2))}{M_2L_2^2 + M_1(L_1 + 2L_2)^2 + 12M_4(L_1 + L_2)^2}\sin\theta_{i1} \tag{3}$$

where g is the acceleration of gravity.

It is assumed that $\theta_{i2} = 0$ during SS, so θ_{i1} is equal to $-\theta_{i3}$ (hip flexion angle equals ankle plantar flexion angle) during the SS. The first term of Eq. (3) is from [6].

2.3. Double stance phase

As shown in Fig. 1(b), the DS starts right after the SS at the HS of one side and ends at the TO of the other side. As shown in Fig. 2(b) and (d), the movements of both legs during the DS are characterized as a series of planar kinematic chain movements in the sagittal plane. This kinematic chain is simplified [4] by assuming that the knee of the front leg is straight during the DS. A series of force and torque balance equations are solved to achieve the equations of motion for the leg movement during the DS (Appendix A in Supplementary materials).

Since the active ankle torque during the DS does not linearly change with the ankle angle [12], the active ankle torque, T_{i32}, is estimated based on the body mass as:

$$T_{i32}(t) = r_{i32}M_0 \tag{4}$$

2.4. Swing phase

As shown in Fig. 1(b), the SW of one side starts and ends at the TO and HS of the same side, respectively. For the SW, the swing leg is characterized as a double-pendulum, with knee and hip joint torques linearly changing with the associated joint angles, as shown in Fig. 2(c). Equations of motion for the double-pendulum are solved by the Euler-Lagrange differential equations [13] and given by:

$$12M_1L_1^2\ddot{\theta}_{i1} + 6M_2L_1^2\ddot{\theta}_{i1} + 3M_2L_1L_2\ddot{\theta}_{i2}\cos(\theta_{i1} - \theta_{i2}) + 3M_2L_1L_2\dot{\theta}_{i2}^2\sin(\theta_{i1} - \theta_{i2}) + 3M_1L_1g\sin\theta_{i1} + 6M_2L_1g\sin\theta_{i1} + 6k_{i13} = 0 \tag{5}$$

$$3M_2L_1L_2\ddot{\theta}_{i1}\cos(\theta_{i1} - \theta_{i2}) + 2M_2L_2^2\ddot{\theta}_{i2} - 3M_2L_1L_2\dot{\theta}_{i1}^2\sin(\theta_{i1} - \theta_{i2}) + 3M_2L_2g\sin\theta_{i2} + 6k_{i23} = 0 \tag{6}$$

The constraint during the SW is that the knee will be locked to straight once the knee flexion angle reaches zero. Similarly, the ankle will be locked to a neutral angle once the ankle flexion angle reaches zero.

2.5. Phases continuity

The angle and angular velocity of each joint (Fig. 1(c)) at time t, $\theta_{ij}(t)$ and $\dot{\theta}_{ij}(t)$, are summarized in an angle state vector and an angular velocity state vector, $\boldsymbol{\theta}_S(t)$ and $\dot{\boldsymbol{\theta}}_S(t)$:

$$\boldsymbol{\theta}_S(t) = \begin{Bmatrix} \theta_{11}(t) \\ \theta_{12}(t) \\ \theta_{13}(t) \\ \theta_{21}(t) \\ \theta_{22}(t) \\ \theta_{23}(t) \end{Bmatrix} \tag{7}$$

$$\dot{\boldsymbol{\theta}}_S(t) = \begin{Bmatrix} \dot{\theta}_{11}(t) \\ \dot{\theta}_{12}(t) \\ \dot{\theta}_{13}(t) \\ \dot{\theta}_{21}(t) \\ \dot{\theta}_{22}(t) \\ \dot{\theta}_{23}(t) \end{Bmatrix} \tag{8}$$

As shown in Fig. 2, these state vectors are transferred from the end of one phase to the start of the next phase to pass the values of angle and angular velocity of each joint. The initial state vectors are defined as the initial conditions of the right SW and left SS, $\boldsymbol{\theta}_S(t_0)$ and $\dot{\boldsymbol{\theta}}_S(t_0)$. By solving the forward dynamics, the end conditions of this phase are calculated

and used as the initial conditions of the next phase. This process continues through all four phases and eventually ends at the start of the right SW and left SS with state vectors as $\boldsymbol{\theta}_S(t_4)$ and $\dot{\boldsymbol{\theta}}_S(t_4)$.

The errors between the initial conditions and end conditions are defined with two error vectors, $\boldsymbol{\varepsilon}_{\boldsymbol{\theta}}$ and $\boldsymbol{\varepsilon}_{\dot{\boldsymbol{\theta}}}$, where each element is the absolute value of differences between the corresponding elements in the state vector at the initial conditions and the associated end conditions:

$$\boldsymbol{\varepsilon}_{\boldsymbol{\theta}} = |\boldsymbol{\theta}_S(t_0) - \boldsymbol{\theta}_S(t_4)| \tag{9}$$

$$\boldsymbol{\varepsilon}_{\dot{\boldsymbol{\theta}}} = |\dot{\boldsymbol{\theta}}_S(t_0) - \dot{\boldsymbol{\theta}}_S(t_4)| \tag{10}$$

2.6. Initial conditions at the right TO

To simplify the state vectors for the initial conditions, several assumptions are made to reduce the dimension of the state vectors. Since the foot in the front and toe of the trailing foot are assumed to be on the ground (Fig. 2(d)) during the DS and at the right TO (start of the gait), the vertical distances between them and the hip joints satisfy:

$$(L_1 + L_2)\cos\theta_{11} + L_4 = L_4\cos(\theta_{22} - \theta_{21} - \theta_{23}) + L_3\sin(\theta_{22} - \theta_{21} - \theta_{23}) + L_2\cos(\theta_{22} - \theta_{21}) - L_1\cos\theta_{21} \tag{11}$$

Thus, the ankle angle and angular velocity of the trailing leg, θ_{23} and $\dot{\theta}_{23}$, can be derived from other joint angles (θ_{11}, θ_{21}, and θ_{22}) and angular velocities ($\dot{\theta}_{11}$, $\dot{\theta}_{21}$, and $\dot{\theta}_{22}$). Also, the leg in the front is assumed straight, and the foot in the front is assumed flat on the ground during the DS and at the right TO (start of the gait):

$$\theta_{12}(t_0) = \dot{\theta}_{12}(t_0) = 0 \tag{12}$$

$$\theta_{13}(t_0) = -\theta_{11}(t_0) \tag{13}$$

$$\dot{\theta}_{13}(t_0) = -\dot{\theta}_{11}(t_0) \tag{14}$$

Thus, the state vectors for the initial conditions can be simplified as:

$$\boldsymbol{\theta}_S(t_0) = \begin{Bmatrix} \theta_{11}(t_0) \\ 0 \\ -\theta_{11}(t_0) \\ \theta_{21}(t_0) \\ \theta_{22}(t_0) \\ \theta_{23}(t_0) \end{Bmatrix} \tag{15}$$

$$\dot{\boldsymbol{\theta}}_S(t_0) = \begin{Bmatrix} \dot{\theta}_{11}(t_0) \\ 0 \\ -\dot{\theta}_{11}(t_0) \\ \dot{\theta}_{21}(t_0) \\ \dot{\theta}_{22}(t_0) \\ \dot{\theta}_{23}(t_0) \end{Bmatrix} \tag{16}$$

where the angle state vector has 3 dimensions, $\theta_{11}(t_0)$, $\theta_{21}(t_0)$, and $\theta_{22}(t_0)$, and the angular velocity state vector has 3 dimensions, $\dot{\theta}_{11}(t_0)$, $\dot{\theta}_{21}(t_0)$, and $\dot{\theta}_{22}(t_0)$. $\theta_{23}(t_0)$ and $\dot{\theta}_{23}(t_0)$ can be derived from other angles and angular velocities based on Eq. (11).

2.7. Sensitivity analysis

A sensitivity analysis was performed using analysis of variance (ANOVA) to investigate the effect of model inputs on outputs. The inputs (independent and subject variables) were $\boldsymbol{\theta}_S(t_0)$, $\dot{\boldsymbol{\theta}}_S(t_0)$, subject stature, L_0, subject body mass, M_0, and subject gender. The outputs (dependent variables) were $\boldsymbol{\varepsilon}_{\boldsymbol{\theta}}$, $\boldsymbol{\varepsilon}_{\dot{\boldsymbol{\theta}}}$, step length, swing time, and stance time.

2.7.1. Range of inputs

The normal range of initial conditions (at TO) for model inputs was determined from the available literature. Reported joint angles and angular velocities in the sagittal plane for the normal gait at TO from 11 publications are summarized in Table 2. The hip flexion angles of the front and trailing legs at TO ranged from 5 to 30° and –30 to –5°, respectively [12,14–19]. The knee flexions of the front and trailing legs ranged from 0 to 20° and 20 to 45°, respectively [12,14,23,15–22]. Some of these studies also reported that the hip flexion angular velocities of the front and trailing legs at TO ranged from –200 to –100° per second and 100 to 150° per second, respectively [18,19]. Tong and Granat [19] reported the observed knee flexion angular velocities of the front and trailing legs were 20° per second and ranged from 100 to 270° per second, respectively. Some investigators reported that ankle flexion angles of the front and trailing legs ranged from –5 to 10° and –45 to 0°, respectively [12,14–16,18,20,22,23]. These studies gave a reference for the normal range of joint angles and angular velocities as inputs for the model.

The sensitivity analysis examined all combinations of inputs within the selected range and calculated the error vectors for each combination. For the initial conditions (Table 1), the first set of combinations examined included $\theta_{11}(t_0)$ from 5 to 30° with steps of 5°, while $\theta_{21}(t_0) = -5°$, $\theta_{22}(t_0) = 20°$, $\dot{\theta}_{11}(t_0) = -50°$ per second, $\dot{\theta}_{21}(t_0) = 100°$ per second, and $\dot{\theta}_{22}(t_0) = 100°$ per second. Then $\theta_{21}(t_0)$ was decreased by 5°, and the same process was applied to $\theta_{11}(t_0)$ from 5 to 30° with 5° steps. This whole process was repeated until all combinations of $\theta_{11}(t_0)$, $\theta_{21}(t_0)$, $\theta_{22}(t_0)$, $\dot{\theta}_{11}(t_0)$, $\dot{\theta}_{21}(t_0)$, and $\dot{\theta}_{22}(t_0)$ were examined. A complete list and explanations of the combinations for initial conditions examined can be found in Appendix B in Supplementary materials.

The model was adjusted with subject-specific parameters of body mass and height, but the lumped muscle parameters were not subject-specific. As summarized in Table 1, the stature and body mass were selected as 1.51, 1.70, and 1.88 m, and 51, 88, and 125 kg to cover the stature and body mass ranged from 5th percentile female to 95th percentile male reported by ANSUR Data [46]. Both genders were examined in this analysis by differentiating the link length ratios and link mass ratios from Drillis and Contini [24]. The lumped muscle parameters were estimated based on joint torques during gait reported by Winter [12]. The model iterated the calculation at 100 Hz (10 milliseconds per frame)

2.7.2. Results

A total of 1,049,760 combinations of initial conditions were examined by the sensitivity analysis. Some combinations did not meet the switching conditions (TOs and HSs) between phases or were physiologically impossible, such as gait with the swing foot landing behind the stance foot, and discarded. The discarded combinations of the initial conditions (at TO) mainly had the following characteristics: 1) had knee angles of the trailing leg less than 25° ($\theta_{22}(t_0) < 25°$) or angular velocities ($\dot{\theta}_{22}(t_0) < 125°$ per second) that resulted in insufficient knee flexion and stubbing toe during SW; and 2) had small (absolute) hip angles of the trailing leg ($\theta_{21}(t_0) < -10°$) or great hip angular velocities of the trailing leg ($\dot{\theta}_{21}(t_0) > 175°$ per second) that resulted in insufficient time for the foot to be lifted at the beginning of swing; 3) had small hip angular velocities of the trailing leg ($\dot{\theta}_{21}(t_0) < 75°$ per second) that resulted in insufficient energy to swing the trailing leg forward.

Only 116,640 combinations resulted in complete gaits and were analyzed. The predicted walking speed ranged from 0.87 to 1.15 m/s, which was within the range reported in Table 2. A series of regressions were performed with the initial conditions as the predictor, and the error vectors and gait parameters as responses to examine how much variation in the responses are explained by each predictor.

The variations in each output explained by input are listed in Table 3. Only the initial angle of the hip of the front leg at initial TO and the hip of the trailing leg at initial TO accounted for more than 1% of the variations in error vectors. None of the initial angular velocities accounted for more than 0.1 % of the variations in error vectors. The error vectors were more sensitive to initial angles with 10 % variations explained

Table 2
Summary of observed joint angles for hip, knee, and ankle, and joint angular velocities for hip and knee at right TO and corresponding walking speeds during the walking gait.

Paper	n	Front leg					Latter leg					Walking speed (m/s)
		Hip		Knee		Ankle	Hip		Knee		Ankle	
		θ_{11} (deg)	$\dot{\theta}_{11}$ (deg/s)	θ_{12} (deg)	$\dot{\theta}_{12}$ (deg/s)	θ_{13} (deg)	θ_{21} (deg)	$\dot{\theta}_{21}$ (deg/s)	θ_{22} (deg)	$\dot{\theta}_{22}$ (deg/s)	θ_{23} (deg)	
Begg et al., 2006 [21]	24			5		–5			30 ~ 45		–30 ~ 0	1.36*
Buczek et al., 2010 [14]	25	25 ~ 30		0 ~ 10		–5 ~ 5	–15 ~ –5		25 ~ 30		–46 ~ –25	
Collins et al., 2009 [15]	10	25		10		5	–10		20		–5	
Eltoukhy et al., 2017 [16]	10	15		10		0			25		–5	1.3**
Kiss et al., 2004 [21]	51			10					45			0.83**
Mills et al., 2007 [22]	10			5		10			45		–25	
Ramakrishnan et al., 1991 [17]	1	30		0			–5		30			
Seel et al., 2014 [23]	1			4		–5			30		–30	
Tadano et al., 2013 [18]	5	20 ~ 30	–200 ~ –100	10 ~ 15		–5 ~ 5	–10 ~ –5	100 ~ 120	30 ~ 50		–20 ~ –10	
Tong et al., 1999 [19]	2	5 ~ 15	–130 ~ –100	15	20		–30 ~ –25	100 ~ 150	20 ~ 30	100 ~ 270		
Winter, 1984 [12]	16	10		20		–5	–15		35		–15	
Range	212	5 ~ 30	–200 ~ –100	0 ~ 20	20	–5 ~ 10	–30 ~ –5	100 ~ 150	20 ~ 45	100 ~ 270	–45 ~ 0	0.83 ~ 1.36

* Self-selected comfort walking speed.
** Preset walking speed on a treadmill.

Table 3
Statistics of the sensitivity analysis outcomes (error vectors and gait parameters) and the percent contributions of variations in outcomes explained by initial state vectors, and anthropometry to variations in error vectors and gait parameters for all 49,572 valid combinations (gait cycles) of initial state vectors.

			$\boldsymbol{\varepsilon}_{\theta_s}$ (deg) $(\theta_{ij}(t_4) - \theta_{ij}(t_0))$						$\boldsymbol{\varepsilon}_{\dot{\theta}_s}$ (deg/s)$(\dot{\theta}_{ij}(t_4) - \dot{\theta}_{ij}(t_0))$						S_L* (m)	T_{SW}* (s)	T_{ST}* (s)
			ε_{11}	ε_{12}	ε_{13}	ε_{21}	ε_{22}	ε_{23}	$\dot{\varepsilon}_{11}$	$\dot{\varepsilon}_{12}$	$\dot{\varepsilon}_{13}$	$\dot{\varepsilon}_{21}$	$\dot{\varepsilon}_{22}$	$\dot{\varepsilon}_{23}$			
Statistics		Mean	0.62	–	0.62	0.75	0.46	0.49	11	–	11	37	35	9.5	0.70	0.31	0.42
		SD	0.41	–	0.41	0.60	0.40	0.58	18	–	18	62	62	19	0.13	0.17	0.27
		Min	0.06	–	0.06	0	0	0	0	–	0	0.3	0.2	0	0.35	0.10	0.21
		Max	2.2	–	2.2	6.2	5.6	2.8	245	–	245	135	970	289	0.76	0.56	1.1
Range of motion during the gait cycle		Max	19	46	13	19	54	18	276	650	245	203	970	289	–	–	–
		Min	−20	0	−16	−23	0	−20	0	0	0	0	0	0	–	–	–
Contribution (%)	Initial conditions	$\theta_{11}(t_0)$	0.3	–	0.3	2.6	3.8	0.1	0.5	–	0.5	7.7	3.5	0.1	62	2.3	2.3
		$\theta_{21}(t_0)$	7.0	–	7.0	14	11	4.0	1.8	–	1.8	5.0	2.2	0.4	16	0	0
		$\theta_{22}(t_0)$	0	–	0	0.1	0.5	0	0	–	0	0.5	0.6	0	6	1.3	1.3
		$\dot{\theta}_{11}(t_0)$	0	–	0	0	0.1	0.1	0	–	0	0.1	0	0.1	0	13	13
		$\dot{\theta}_{21}(t_0)$	0	–	0	0	0	0	0	–	0	0	0	0	0	6.3	6.2
		$\dot{\theta}_{22}(t_0)$	0	–	0	0	0	0	0	–	0	0	0	0	0	7.0	6.8
	Anthropometry	Gender	0	–	0	0	0	0	0	–	0	0	0	0	0	0	0
		L_0	0	–	0	0	0	0	0	–	0	0	0	0	12	1	2
		M_0	0	–	0	0	0	0	0	–	0	0	0	0	3	3	2

* S_L is step length, T_{SW} is swing time, and T_{ST} is stance time (SS + DS).

compared with initial angular velocities. The variations in subject stature explained 12 % of variations in step length.

2.7.3. Sample joint kinematics

As shown in Fig. 3, the sample predicted joint angles, angular velocities, and angular accelerations during one gait cycle were compared with the values reported by Winter [12]. The overall trends of angles, angular velocities, and angular accelerations were consistent between the predicted and reported values except for the hip angular accelerations during the DS.

In total, seven typical instances with discontinuity in angular accelerations were identified. H1 and H2 were two instances at phase transitions between DS and SW, and SW and DS, with means and standard deviations of $1092 \pm 298°/s^2$ and $582 \pm 274°/s^2$, respectively, among all the examined gait cycles. K1 and K2 were two instances at the phase transition between SS and DS, and near the end of SW, with means and standard deviations of $3805 \pm 401°/s^2$ and $6661 \pm 614°/s^2$, respectively, among all the examined gait cycles. A1, A2, and A3 were three instances at the phase transition between SS and DS, during SW, and at the phase transition between SW and DS, with means and standard deviations of $10432 \pm 935°/s^2$, $5016 \pm 358°/s^2$, and $5983 \pm 1538°/s^2$, respectively, among all the examined gait cycles.

2.8. Global error vector and optimization problem

A global error vector, $\boldsymbol{E}$, is proposed in this work to quantify the gait discontinuity and compare the overall error resulting from different initial conditions. The global error vector's s^{th} element is:

$$\boldsymbol{E}(s) = ||\boldsymbol{\varepsilon}_{\boldsymbol{\theta}}^{s}|| + f||\boldsymbol{\varepsilon}_{\dot{\boldsymbol{\theta}}}^{s}|| \quad (17)$$

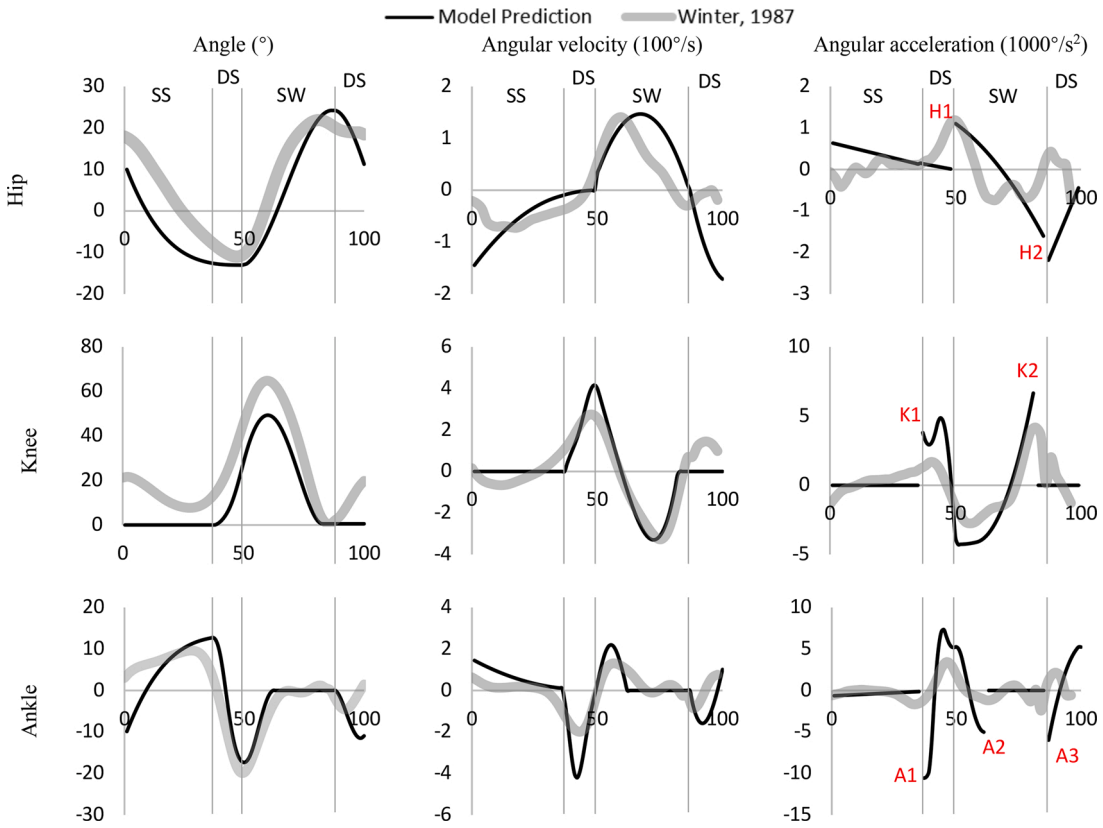

Fig. 3. Sample joint angles, angular velocities, and angular accelerations of hip, knee, and ankle compared with values reported by Winter [25] versus percent of the gait cycle. H1 and H2 are the instances where the discontinuity of hip angular acceleration occurs during gait, K1 and K2 are the instances where the discontinuity of knee angular acceleration occurs during gait, and A1, A2, and A3 are the instance where discontinuity of ankle angular acceleration occurs.

where s is the order of the initial conditions being examined, $||\boldsymbol{\varepsilon}_{\theta}^{s}||$ is the norm of the angle error vector for the s^{th} initial conditions, $||\boldsymbol{\varepsilon}_{\dot{\theta}}^{s}||$ is the norm of the angular velocity error vector for the s^{th} initial conditions, and f is a scalar factor used to adjust the weighing between errors in angles and angular velocities.

To achieve periodic gait, as shown in Fig. 2, the end conditions of a gait cycle should be equal to the initial conditions of that gait cycle to maintain continuity and consistency between phases and gait cycles. An optimization problem is formed with the objective to minimize the global error of the predicted gait cycle with initial conditions as variables and the dynamic systems of gait phases as constraints. The model enumerates a range of initial conditions and utilizes forward dynamics to calculate the end conditions and global errors to find the optimal initial conditions that could lead to minimum global error, or gait discontinuity.

3. Discussion

3.1. Constraints and assumptions

The physical constraint added to the model was end conditions equal to initial conditions, or periodic gaits. The global error vector was minimized to satisfy this constraint. Based on the sensitivity analysis result (Table 3), the errors between initial and end conditions were mostly sensitive to initial joint angles other than initial joint angular velocities. Thus, the scalar factor in the global error vector should be less than 1 to accommodate this effect. Physiologically, this meant the continuity of body posture was more important than the continuity of the kinetic energy during gait.

The major assumption of the proposed model was that the front leg was initially straight (knee flexion angle = 0°) at the beginning of the DS and SS. Most of the literature reported less than 10° in knee flexion during the DS and SS (Table 2). Compared with a straight knee, 10° in knee flexion would only result in a 1.5 % reduction in the length of the front leg and about 1% reduction in stance time and step length, which was considered negligible in this model. Furthermore, a specific knee angle at TO can be assumed for gait simulation with the model for future investigation to compensate according to the individual's gait pattern.

$$\boldsymbol{E}(s) = ||\boldsymbol{\varepsilon}_{\theta}^{s}|| + f||\boldsymbol{\varepsilon}_{\dot{\theta}}^{s}||$$

3.2. Limitations and future works

The PPCLMP model had four major limitations: simplified representations of joints and body segments, spring representation of muscles, discontinuity in angular acceleration, and constant lumped muscle parameters. The model simplified the representations of joints and body segments to one degree of freedom hinge joints and rod links with uniformly distributed masses. However, females and drop foot patients tend to have more hip abduction during gait [25,26], which is not captured by the current model. Significant hip abduction could result in a longer swing and shorter step length due to the nature of the conic pendulum [27]. In addition, the rotation of the pelvis was omitted, which could cause the predicted gait to be more fluctuated and shorter in step length [8]. The proposed model was simplified into 2-D in this paper to meet the goal of developing a model to utilize inputs available in clinical or home settings. As future work, 3D elements can be added to develop the model to a quasi-3D model. More efforts are needed to explore approaches to simplify the lateral inertia of body segments, including the upper body, that need to be involved to maintain the lateral balance. In addition, human legs do not have uniformly distributed masses [28]. Different representations of joints and body segments should be explored with the model for future development.

The lumped muscle parameters for the knee and hip joints were proposed based on the rotational spring representation of related muscles. This representation was simplified from Hill's muscle model [29] that has a contractile element and two spring elements. The viscoelasticity of muscles can be further represented by adding damping factors to the spring element. The exclusion of the viscoelasticity of muscles in this study was aimed to reduce the dimensions of variables in the model but could introduce errors to the model prediction. Without considering the viscoelasticity, the dynamic system in the model tends to move faster and has less energy loss.

The angular accelerations of hip, knee, and ankle joints were instantaneously changed during gait cycles (Fig. 3), while reported values from Winter [12] and the nature of human walking suggest that the accelerations and forces during gait cycles are continuous. This may indicate one of the limitations of the model is that the model-predicted gait cycles tend to have more dramatic force changes during phase transition. One possible solution is to create several frames (10 milliseconds per frame) as transition frames between phases. During transition frames, the acceleration will continuously change from the value at the end of the previous phase to the value at the beginning of the next phase. Though with this limitation, the model predicted joint angles and angular velocities follow the trend of reported values.

The observed inconsistencies of hip angular acceleration during DS between the predicted and reported values can be explained by the ankle torque in the PPCLMP model. The model imposes a sudden change of torque of the push-off ankle at the beginning of DS, while the ankle torque increases gradually for real gait. This difference causes the required torque of the hip of the trailing leg to be less in the model prediction to move the body forward during the first DS in Fig. 3. Similarly, the torque of the hip of the front leg (second DS in Fig. 3) is greater in the model prediction to compensate for the sudden increase of ankle torque of the other leg.

While most of the discontinuity occurred at phase transitions due to the different mechanical properties of different dynamic systems of different phases, K2 and A2 instances in Fig. 3 did not normally occur at the phase transition, but during SW. These are due to the constraints of SW that the knee and ankle joint angles will be locked once reach neural.

The other limitation of this model was the assumption of generic joint torque patterns for different people (gender, age, impairment, etc.) walking under different environments for different tasks. The generic joint torque patterns assumption ignores the adjustments, adaptions, and preferences of individuals among different scenarios. For example, walking on an inclined ramp or with assistive devices (e.g. ankle-foot orthosis) could involve different joint torque patterns and different dynamic system states, like velocities and angles. However, the model only adapted the dynamic system states to look for a feasible solution without changing the joint torque patterns. In other words, the model may overestimate the effect of assistive devices on gait. Furthermore, the model is limited to predict impaired gait that could have various muscle strength and activity from normal gait. How to determine the correct lumped muscle parameters in the model to make the prediction more individualized is challenging.

3.3. Model modification for pathological gait and assistive devices

The lumped muscle parameters in the PPCLMP model can be modified to simulate motor control issues at a lower-limb joint or the effect of assistive devices. For example, a drop foot patient may have significantly less strength in the dorsiflexors or significantly larger strength in the plantar flexors (e.g. spasticity) of the ankle joint. Wearing assistive devices can also be simulated by adding the mechanical property of the assistive device to the lumped muscle parameter to estimate the joint torque for the forward dynamic calculations.

3.4. Vision of integrating IMU measurements into the PPCLMP model

As popular gait tracking wearable devices, IMUs have advantages in their accuracy, less intrusive, and robustness in challenging environments [23]. One IMU on the shank (or assistive devices attached to the shank) can measure the accelerations and angular velocities of the shank during the entire gait cycle. Similar to the approach of well-reviewed inverse kinematic models [30], these kinematic measurements can be used as the constraints in the proposed optimization problem to predict cyclical gait that also matches the IMU measurements of one shank. With more constraints added, lumped muscle parameters can be changed from generic parameters into variables of the optimization problem to help determine individual lumped muscle parameters to improve and customize the gait prediction. Further investigations are needed to evaluate the IMU-assisted prediction.

4. Conclusions

This work proposes a PPCLMP model that links together existing inverted pendulum, kinematic chain, and double pendulum models to predict lower limb posture and movement across the entire gait cycle by simplifying muscle forces into lumped muscle parameters. This model is based on physical constraints of periodic gait that require the initial point of each phase to be determined by the end point of the previous phase. This work shows the PPCLMP model is able to predict gait cycles by using initial conditions within a certain range and minimize the error between initial and end conditions of a gait cycle based on forward dynamics. This work also explores the range of initial conditions, especially the initial condition of the knee and hip of the trailing leg at TO, within which the model works.

With the 2-D representations of lower limbs and simplified representations of joint torques, the model only takes anthropometry data and generic lumped muscle parameters to predict gait cycles. The model builds the foundation of gait assessment tools using inputs from simple motion tracking tools (e.g. IMUs) available at clinics.

Declaration of Competing Interest

The authors report no declarations of interest.

Acknowledgments

This work was supported by the National Science Foundation PFI: BIC (Grant 1534003), the National Center for Defense Manufacturing and Machining and America Makes (NCDMMFA8650-12-2-7230), and the Blue Cross Blue Shield of Michigan Foundation (Grant 2158.ii).

Appendix A. Supplementary data

Supplementary material related to this article can be found, in the online version, at doi:https://doi.org/10.1016/j.gaitpost.2021.05.021.

References

[1] G.F. Harris, J.J. Wertsch, Procedures for gait analysis, Arch. Phys. Med. Rehabil. (1994), https://doi.org/10.1016/0003-9993(94)90399-9.
[2] S.L. Dockstader, M.J. Berg, A.M. Tekalp, Stochastic kinematic modeling and feature extraction for gait analysis, IEEE Trans. Image Process. (2003), https://doi.org/10.1109/TIP.2003.815259.
[3] T. Orhanli, A. Yilmaz, Analysis of gait dynamics with the double pendulum model, 27th Signal Process. Commun. Appl. Conf. SIU 2019 (2019), https://doi.org/10.1109/SIU.2019.8806587.
[4] Z. Svoboda, M. Janura, P. Kutilek, E. Janurova, Relationships between movements of the lower limb joints and the pelvis in open and closed kinematic chains during a gait cycle, J. Hum. Kinet. (2016), https://doi.org/10.1515/hukin-2015-0168.
[5] A.D. Kuo, J.M. Donelan, A. Ruina, Energetic consequences of walking like an inverted pendulum: step-to-step transitions, Exerc. Sport Sci. Rev. (2005), https://doi.org/10.1097/00003677-200504000-00006.

[6] M. Srinivasan, A. Ruina, Computer optimization of a minimal biped model discovers walking and running, Nature (2006), https://doi.org/10.1038/nature04113.
[7] M. Ackermann, A.J. van den Bogert, Optimality principles for model-based prediction of human gait, J. Biomech. (2010), https://doi.org/10.1016/j.jbiomech.2009.12.012.
[8] L. Ren, R.K. Jones, D. Howard, Predictive modelling of human walking over a complete gait cycle, J. Biomech. (2007), https://doi.org/10.1016/j.jbiomech.2006.07.017.
[9] A.I. Mahyuddin, S. Mihradi, T. Dirgantara, A. Sukmajaya, N. Juliyad, U. Purba, Development of an affordable system for 2D kinematics and dynamics analysis of human gait, Fourth Int. Conf. Exp. Mech. (2009), https://doi.org/10.1117/12.851654.
[10] A.H. Hansen, D.S. Childress, E.H. Knox, Roll-over shapes of human locomotor systems: effects of walking speed, Clin. Biomech. (2004), https://doi.org/10.1016/j.clinbiomech.2003.12.001.
[11] C.C. Gordon, T. Churchill, C.E. Clauser, J.T. Mcconville, I. Tebbetts, R.A. Walker, 1988 anthropometric survey of U.S. Army personnel: Methods and summary statistics, Security (2012) 640.
[12] D.A. Winter, Kinematic and kinetic patterns in human gait: variability and compensating effects, Hum. Mov. Sci. (1984), https://doi.org/10.1016/0167-9457(84)90005-8.
[13] V.I. Arnold, V.V. Kozlov, A.I. Neishtadt, Variational Principles and Methods, 2006, https://doi.org/10.1007/978-3-540-48926-9_4.
[14] F.L. Buczek, M.J. Rainbow, K.M. Cooney, M.R. Walker, J.O. Sanders, Implications of using hierarchical and six degree-of-freedom models for normal gait analyses, Gait Posture (2010), https://doi.org/10.1016/j.gaitpost.2009.08.245.
[15] T.D. Collins, S.N. Ghoussayni, D.J. Ewins, J.A. Kent, A six degrees-of-freedom marker set for gait analysis: repeatability and comparison with a modified Helen Hayes set, Gait Posture (2009), https://doi.org/10.1016/j.gaitpost.2009.04.004.
[16] M. Eltoukhy, J. Oh, C. Kuenze, J. Signorile, Improved kinect-based spatiotemporal and kinematic treadmill gait assessment, Gait Posture (2017), https://doi.org/10.1016/j.gaitpost.2016.10.001.
[17] H.K. Ramakrishnan, M.P. Kadaba, On the estimation of joint kinematics during gait, J. Biomech. (1991), https://doi.org/10.1016/0021-9290(91)90175-M.
[18] S. Tadano, R. Takeda, H. Miyagawa, Three dimensional gait analysis using wearable acceleration and gyro sensors based on quaternion calculations, Sensors (Switzerland) (2013), https://doi.org/10.3390/s130709321.
[19] K. Tong, M.H. Granat, A practical gait analysis system using gyroscopes, Med. Eng. Phys. (1999), https://doi.org/10.1016/S1350-4533(99)00030-2.
[20] R.K. Begg, W.A. Sparrow, Ageing effects on knee and ankle joint angles at key events and phases of the gait cycle, J. Med. Eng. Technol. (2006), https://doi.org/10.1080/03091900500445353.
[21] R.M. Kiss, L. Kocsis, Z. Knoll, Joint kinematics and spatial-temporal parameters of gait measured by an ultrasound-based system, Med. Eng. Phys. (2004), https://doi.org/10.1016/j.medengphy.2004.04.002.
[22] P.M. Mills, S. Morrison, D.G. Lloyd, R.S. Barrett, Repeatability of 3D gait kinematics obtained from an electromagnetic tracking system during treadmill locomotion, J. Biomech. (2007), https://doi.org/10.1016/j.jbiomech.2006.06.017.
[23] T. Seel, J. Raisch, T. Schauer, IMU-based joint angle measurement for gait analysis, Sensors (Switzerland) (2014), https://doi.org/10.3390/s140406891.
[24] R. Drillis, R. Contini, Segment length expressed as ratio of body height, New York Off. Vocat. Rehabil. (1966).
[25] S.H. Cho, J.M. Park, O.Y. Kwon, Gender differences in three dimensional gait analysis data from 98 healthy Korean adults, Clin. Biomech. (2004), https://doi.org/10.1016/j.clinbiomech.2003.10.003.
[26] R. Don, M. Serrao, P. Vinci, A. Ranavolo, A. Cacchio, F. Ioppolo, M. Paoloni, R. Procaccianti, F. Frascarelli, F. De Santis, F. Pierelli, M. Frascarelli, V. Santilli, Foot drop and plantar flexion failure determine different gait strategies in Charcot-Marie-Tooth patients, Clin. Biomech. (2007), https://doi.org/10.1016/j.clinbiomech.2007.06.002.
[27] K. Dean, Conical pendulum: part 2 a detailed theoretical and computational analysis of the period, tension and centripetal forces, Eur. J. Phys. Educ. 8 (2017) 11–30.
[28] J.L. Durkin, J.J. Dowling, Body segment parameter estimation of the human lower leg using an elliptical model with validation from DEXA, Ann. Biomed. Eng. (2006), https://doi.org/10.1007/s10439-006-9088-6.
[29] A. Hill, The heat of shortening and the dynamic constants of muscle, Proc. R. Soc. Lond. Ser. B Biol. Sci. (1938), https://doi.org/10.1098/rspb.1938.0050.
[30] S.J. Zadeh, A. Khosravi, A. Moghimi, N. Roozmand, A review and analysis of the trajectory gait generation for humanoid robot using inverse kinematic, ICECT 2011 - 2011 3rd Int. Conf. Electron. Comput. Technol. (2011) 358–362, https://doi.org/10.1109/ICECTECH.2011.5942115.